Identifying High-Water Marks in Post-Disaster Reconnaissance Using Multispectral Imagery

Michael H. Gardner, Ph.D., P.E., M.ASCE¹; Elliot Nichols, S.M.ASCE²; Nina Stark, Ph.D., A.M.ASCE³; Anne Lemnitzer, Ph.D., A.M.ASCE⁴; and J. David Frost, Ph.D., P.E., F.ASCE⁵

¹Dept. of Civil and Environmental Engineering, Univ. of California, Davis, CA.

Email: mhgardner@ucdavis.edu

²School of Civil and Environmental Engineering, Georgia Institute of Technology, Atlanta, GA.

Email: enichols9@gatech.edu

³Dept. of Civil and Environmental Engineering, Virginia Tech, Blacksburg, VA.

Email: ninas@vt.edu

⁴Dept. of Civil and Environmental Engineering, Univ. of California, Irvine, CA.

Email: alemnitz@uci.edu

⁵School of Civil and Environmental Engineering, Georgia Institute of Technology, Atlanta, GA.

Email: david.frost@ce.gatech.edu

ABSTRACT

Flooding annually causes thousands of fatalities and billions of dollars in damage globally, while predicting future floods has become increasingly challenging due to changing urban environments and land surface conditions. Furthermore, due to climate change and associated shifts in rain patterns, severe floods are likely to increase. High-water marks collected post-flooding provide key information for advancing our understanding of flood impacts and developing mitigation strategies. However, collecting high-water marks after a flooding event can be complicated due to access issues related to destroyed infrastructure, and detecting high-water marks becomes increasingly difficult with time passing after a flood event. This leads to significant loss of data or risk to personnel entering these recently flooded areas. Here, we present initial data demonstrating the use of multispectral imagery in rapidly collecting and mapping high-water marks post-flooding for different commonly used building materials. This work builds on the exploratory deployment of multispectral imagery during the Geotechnical Extreme Event Association (GEER) response to the July 14, 2021, Western European flood. Additional images were collected in a controlled lab setting to test these initial observations and the potential to extract high-water marks using multispectral imagery of materials commonly used in building façades. These materials included clay bricks, plywood, maple and pine planks, concrete, and steel. Materials were soaked for 48 h after which images were collected at predetermined specific time intervals to establish if and how the signal associated with the high-water mark evolved. For all materials, with the exception of steel, the high-water mark was clearly expressed in the multispectral imagery. Specifically, the blue band (wavelength 465-485 nm) and red-edge band (wavelength 712–722 nm) show the clearest manifestation. Current research is focusing on how the high-water mark can be significantly enhanced and clearly identified through linear combinations of spectral bands. This will enable the development of material-specific indices for rapidly mapping spatially varying flood depths and extents in urban areas during post-disaster reconnaissance. Furthermore, follow-on testing will use sediment-laden water such that the influence of soil adhering to structure surfaces can be incorporated into identifying high-water marks on various structure and foundation surfaces.

INTRODUCTION

Flooding causing extensive damage, death, and disruption and accounts for approximately 80-90% of documented natural disasters (CRED 2021). The recent flooding in western Europe in July 2021 serves as an example of the risk posed by extreme flooding. Over 230 people died, and flood-related damage is estimated to be on the order of 54 billion Euros (Munich Re 2022), making this event the most destructive flooding Europe has experienced in the 21st century. Rainfall volume in some areas was estimated to have reached 240 L/m², which is an amount that typically would occur over an entire year, and localized high-water measurements were as high as 11.75 m above the river water level at the time of measurment.

Pre-flood risk assessment and post-flood management require accurate assessment of flooding hazard and resulting damage. Information collected during post-disaster reconnaissance provide pertinent information both in terms of information required for immediate response and emergency management as well as data relevant to long-term hazard assessment and mitigation. Reconnaissance efforts, such as those deployed through GEER, are critical in collecting and preserving perishable information following natural hazard events that can inform emergency response planning and disaster mitigation for future events. As part of these reconnaissance missions, remote sensing and on-ground imaging have become essential in quickly and safely collecting perishable data related to rapid-onset natural hazards, such as floods, cyclones and other windstorms, earthquakes, landslides, wildfires, and volcanic eruptions (Kucharczyk and Hugenholtz 2021; Twigg 2004).

While remote sensing significantly improves the ability to quickly and safely collect various forms of data, mapping high-water marks on structures or other natural features still requires direct measurement by personnel on the ground. This presents challenges in post-disaster reconnaissance as some areas may not be immediately accessible due to unsafe conditions, so surveyors cannot physically access locations to collect this data. This can lead to loss of high-water marks due to drying, repair works, or other environmental impacts.

Recently, multispectral imagery has been shown to have promise in automatically identifying high-water marks on structures such that this key information can be safely obtained during post-disaster reconnaissance (Gardner et al. 2023). It was shown that the flooding high-water mark could be identified in multispectral images collected approximately 3-4 weeks after flooding occurred based on reflectance characteristics of the building façade. However, imagery only included sampling of one building with a façade comprised of plaster-like material and it was not clear whether this signal would be present in other buildings that had façades comprised of different building materials.

In this work, we present initial findings on using multispectral imagery to identify flooding high-water marks on several building materials commonly used in building façades. These materials include clay bricks, plywood, maple and pine planks, concrete, and steel. Materials were soaked for 48 hours after which images were collected at specific time intervals to establish if and how the signal associated with the high-water mark evolved. This approach potentially could be broadly applied in post-flooding reconnaissance to rapidly generate estimates of water elevations, and thus, flooding severity and extent. The remainder of this paper is organized as follows: The procedure for how the materials were prepared and how images were collected is briefly presented, followed by a brief description of how images were processed to show the signal associated with the high-water mark. This is followed by a discussion of the results and conclusions, including potential applications of the results presented in this paper.

DATA COLLECTION AND PROCESSING

Sample Preparation and Image Collection. Seven samples of six common façade materials—clay brick, plywood, maple and pine planks, concrete with and without an epoxy treatment, and steel—were kept at room temperature for multiple days and then photographed using a Micasense Altum Multispectral Camera. The camera records five, high-resolution spectral bands: Blue (465 - 485 nm), Green (550 - 570 nm), Red (663 - 673 nm), Red-Edge (712 - 722 nm), Near-Infrared (820 - 860 nm). Additionally, it records thermal images (8 - 14 μm), albeit at a lower resolution than the other images.

This initial photograph represents the "pre-flood" condition, as shown in Figure 1. In this figure, the reflectance for each material in the Red-Edge band is shown as an example. Similar images are generated for each of the other spectral bands recorded by the camera. After this initial sample preparation and image collection, sample materials were then submerged to approximately half their total height in tap water for 48 hours. Immediately following the removal of the samples from the water, multispectral images were collected at pre-determined time intervals. The time intervals of the photos after removal from the water were as follows: 1 min., 5 min., 15 min., 30 min., 1 hr., 2 hrs., 4 hrs., 8 hrs., 24 hrs., and 48 hrs. Figures 2 and 3 show the reflectance of the specimens at 1 min. and 48 hrs.

Image Processing. Raw image pixel values must be converted to undistorted reflectance. The details of this procedure are outlined in Gardner et al (2023), as briefly described below. In order to compare images taken at different times and varying incoming solar radiation, it is necessary to convert the digital number pixel values from the multispectral imagery to reflectance values. As a first step, raw pixel values must be converted to absolute spectral radiance, *L*. For the Micasense sensors used in this work, this is done as follows (MicaSense, 2022):

$$L = V(x, y) \cdot \frac{a_1}{g} \cdot \frac{p - p_{BL}}{t_e - a_2 y - a_3 t_e y}$$

where p is the normalized digital number pixel value; p_{BL} is the normalized black level value; a_1 , a_2 , and a_3 are radiometric calibration coefficients; V(x,y) is the vignette polynomial function for a pixel located at location (x, y); t_e is the image exposure time; and g is the sensor gain setting. The values for these parameters are read from the image metadata and the MicaSense sensors use a radial vignette model defined as:

$$V(x,y) = \frac{1}{k}$$

where

$$k = 1 + k_0 r + k_1 r^2 + k_2 r^3 + k_3 r^4 + k_4 r^5 + k_5 r^6$$
$$r = \sqrt{(x - c_x)^2 + (y - c_y)^2}$$

where c_x , c_y , and the polynomial coefficients k_1 through k_5 are read from the image metadata. In order to calculate reflectance values for each pixel, a transfer function for each of the spectral

bands is calculated based on the average radiance of pixels in an image taken of a calibrated reflectance panel (MicaSense 2022):

$$F_i = \frac{\rho_i}{\overline{L}_i}$$

where F_i is the radiance-to-reflectance factor for band i; ρ_i is the reflectance value for the calibrated panel for band i; and \overline{L}_i is the mean radiance of pixels on the calibrated panel area for band i. Calibrated panel images were taken just prior to each of the timed image collections to ensure calibration accounts for potentially changing light conditions during image collection. Based on these conversions and calibrated transfer functions, the calculated undistorted reflectances are what is shown in Figures 1 through 3.

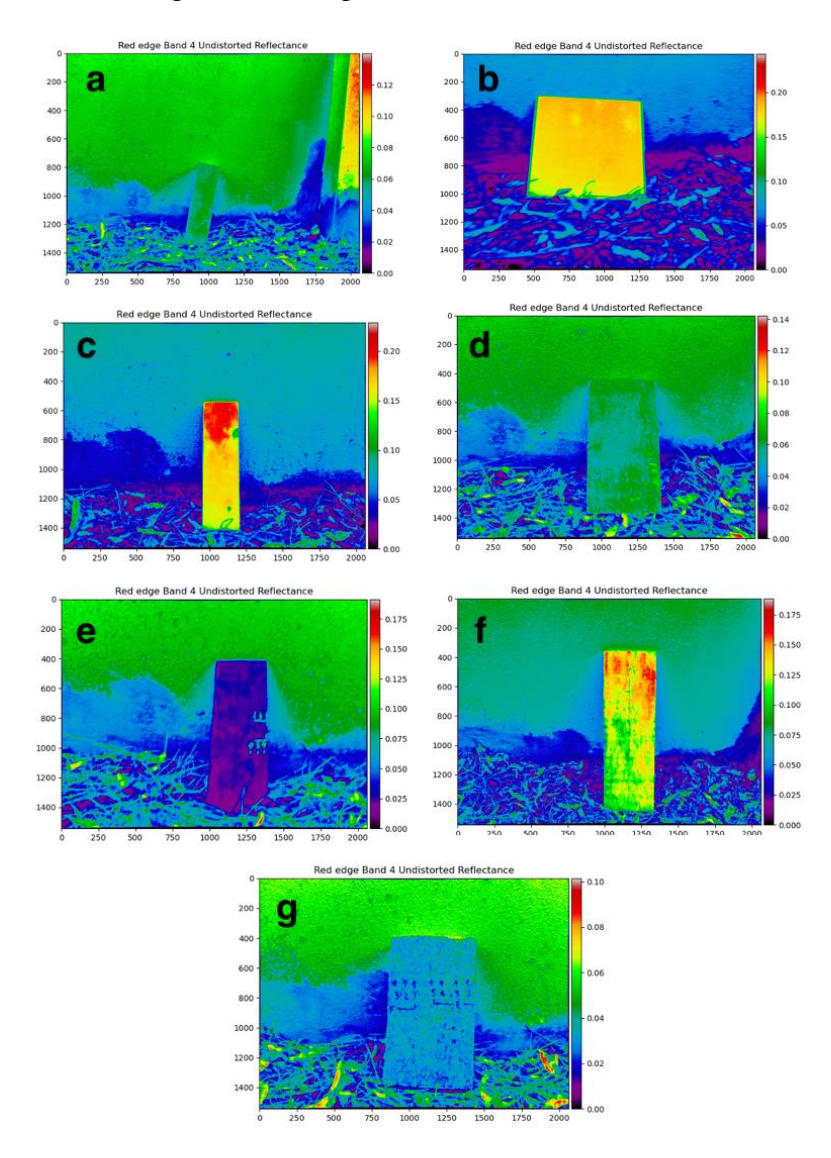


Figure 1. Initial, "Pre-Flood" Red-Edge band reflectance of seven different materials commonly used in façade construction: a) Clay brick; b) Plywood; c) Maple; d) Concrete without epoxy; e) Steel; f) Pine; g) Concrete with epoxy

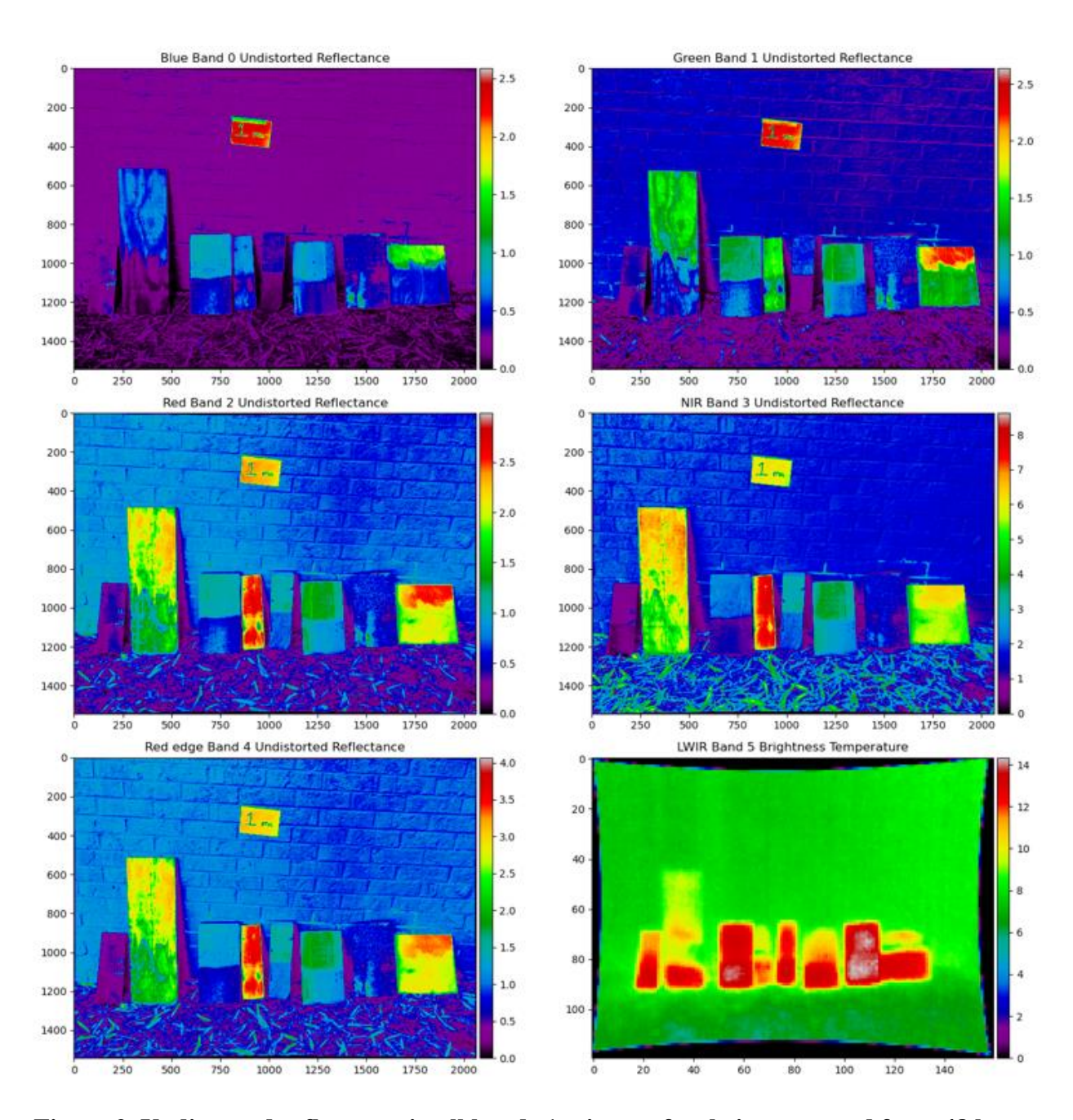


Figure 2. Undistorted reflectance in all bands 1 minute after being removed from 48 hours of soaking in water. Material specimens from left to right: steel, pine, concrete with no epoxy, maple, clay brick, concrete with no epoxy, concrete with epoxy, plywood.

RESULTS AND DISCUSSION

The initial results presented here promise the potential of using multispectral imagery for post-flood high-water mapping across a broad range of commonly used building materials that are present in building façades. This can be seen most clearly in Figure 2 where the high-water mark is clearly visible on all materials with varying strength across all bands. As the time after removal of the samples from water increases, the signal strength decreases although the high-

water mark is still quite clear, particularly in the blue and green bands. The signal strength is strongest in materials that are more porous; this is likely due to the higher presence of water remaining in the pores of materials such as wood or concrete.

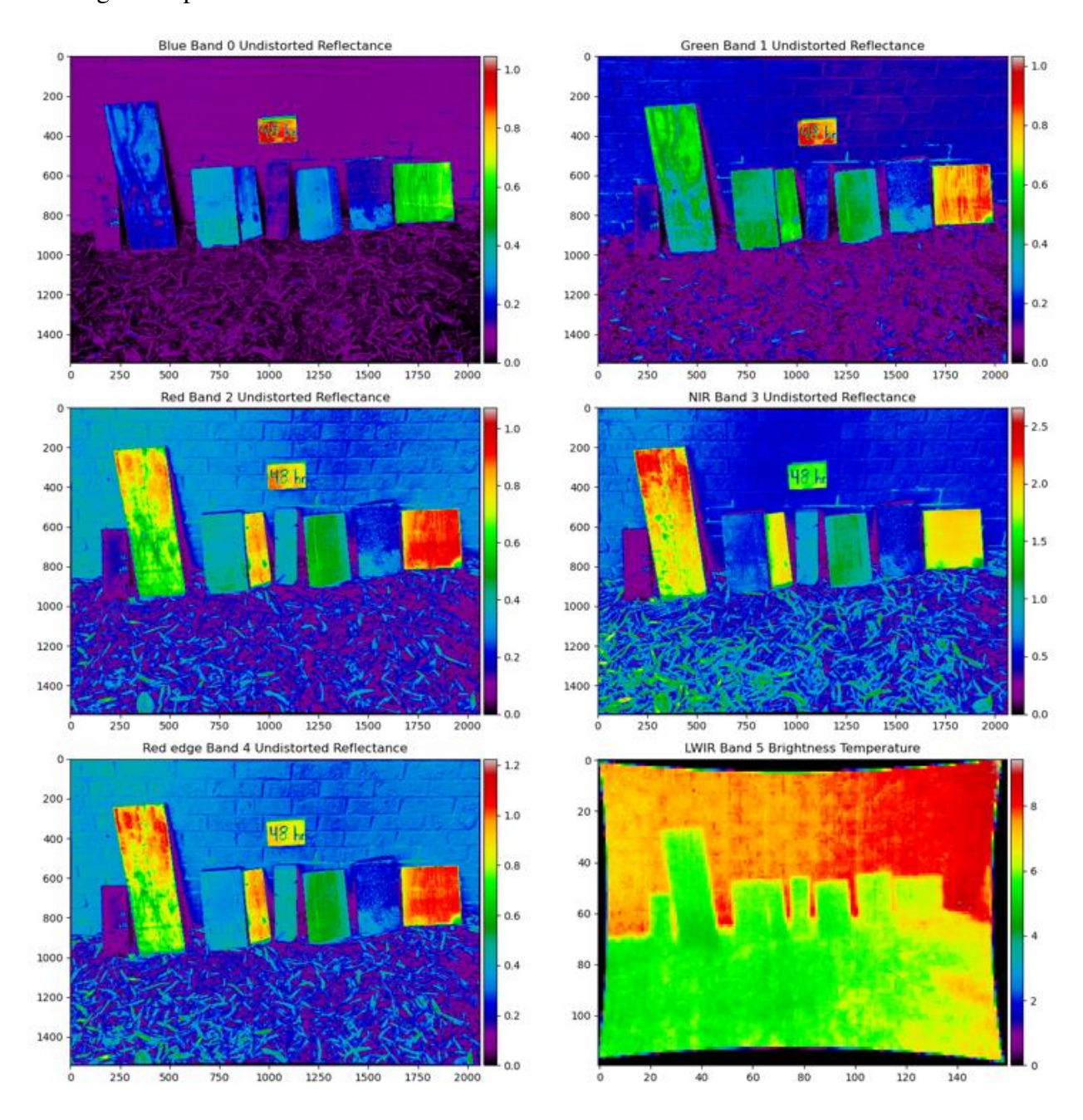


Figure 3. Undistorted reflectance in all bands 48 hours after being removed from 48 hours of soaking in water. Material specimens from left to right: steel, pine, concrete with no epoxy, maple, clay brick, concrete with no epoxy, concrete with epoxy, plywood.

Given these initial images, combinations of different bands would ideally be explored to isolate the signal associated with the high-water mark. This could be done using, for example, the normalized difference between the Red-Edge and Blue bands (NDRE-B) (Gardner et al, 2023).

This may highlight differences in how the high-water manifests in different building materials such that specific band combinations can be identified to isolate this signal in various building façades during post-disaster reconnaissance. However, the images presented here were collected relatively close-up to the material samples, which presents issues in aligning the images from the different bands so that spectral indices can be calculated on a pixel-by-pixel basis. When the images are collected too close to the image subject, the offset between the images from the samples bands becomes sufficiently large such that aligning images results in distortion of the co-aligned, clipped image, as shown in Figure 4. Thus, careful consideration must be given to the camera to subject distance in the event that spectral index calculations are of interest.

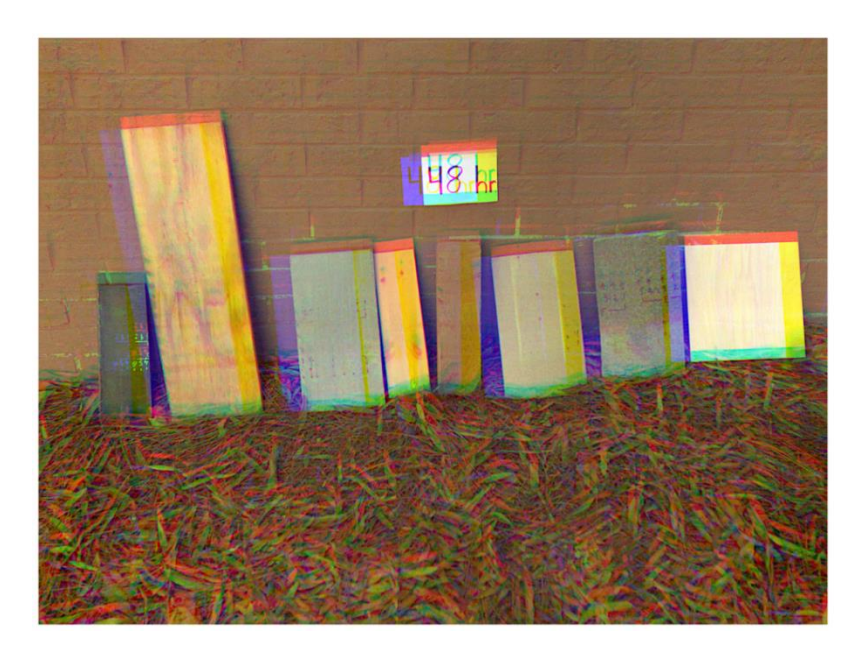


Figure 4. True-color composite images created by combining Red, Blue, and Green Band images. Note color distortion in composite image due to small camera-subject distance. Material specimens from left to right: steel, maple, clay brick, concrete with no epoxy, pine, concrete with no epoxy, concrete with epoxy, plywood.

While the camera-subject distance in this preliminary set of images precludes the calculation of spectral indices on co-aligned pixels, it still is possible to calculate average reflectance values across specific regions of the images which can be combined to provide averaged spectral index values. This approach is currently being explored as a means to evaluate the evolution and degradation of the signal associated with the high-water mark.

CONCLUSION

The challenges posed by evolving extreme flooding hazard require a means by which to quickly, effectively, and safely map the extent of flooding levels and associated damage caused by it. High-water marks are key information in terms of describing the spatially varying depth and extent of flooding that need to be collected during post-disaster reconnaissance. Given the difficulty in accessing areas impacted by flooding, it is necessary to develop techniques that can detect high-water marks days to weeks after flooding occurs.

Our preliminary results build on the findings of Gardner et al (2023) in exploring the application of multispectral imagery in quickly and safely identifying high-water marks. The high-water mark can be visually identified in the undistorted reflectance images of different commonly used building materials, albeit with different levels of strength that depend on the porosity of the soaked material. Additionally, the characteristics of the presence of the high-water mark in the multispectral images changes based on the time since the material was removed from water.

Further work is required to explore how this signal can be isolated in different building materials. This will require images to be taken far enough away from the material samples so that images from all sampled bands can be aligned to allow for pixel-by-pixel index calculations. Additionally, a sufficiently large amount of data needs to be collected so that the presence and variability of the signal associated with the flooding high-water mark can be statistically assessed. Furthermore, follow-on testing should use sediment laden water such that the influence of soil adhering to structure surfaces can be incorporated into identifying high-water marks on various structure and foundation surfaces. Ultimately, this approach can consider the combined use of ground-based and UAV-based image collection.

ACKNOWLEDGMENTS

This research was supported by the National Science Foundation (NSF) through award CMMI-2213768, -2213715, -2213714. Data was collected in part using instrumentation provided by the NSF as part of the RAPID Facility, a component of the Natural Hazards Engineering Research Infrastructure, under Award No. CMMI-2130997. Additional support was provided by NSF through award CMMI-1826118 to the GEER Association.

REFERENCES

- CRED (Centre for Research on the Epidemiology of Disaster). (2021). *Disaster year in review* 2020: Global trends and perspectives. Brussels, Belgium: Université Catholique de Louvain.
- Gardner, M., Nichols, E., Stark, N., Lemnitzer, A., and Frost, D. (2023). "Multispectral Imaging for Identification of High-Water Marks in Postdisaster Flood Reconnaissance". *Natural Haz*ards Review, 24(2), 06023002.
- Kucharczyk, M., and Hugenholtz, C. H. (2021). "Remote sensing of natural hazard-related disasters with small drones: Global trends, biases, and research opportunities." *Remote Sens. Environ.* 264 (14): 112577.
- MicaSense. (2022). "Radiometric calibration model for MicaSense sensors." Accessed August 1, 2022. https://support.micasense.com/hc/en-us/articles/115000351194-Radiometric-Calibration-Model-for-MicaSense -Sensors.
- Munich Re. (2022). "Factsheet natural catastrophes in 2021." Accessed May 1, 2023. https://www.munichre.com/content/dam/munichre/mrwebsiteslaunches/natcat-2022/2021_Figures-of-the-year.pdf/_jcr_content/renditions/original./2021_Figures-of-the-year.pdf.
- Twigg, J. (2004). Disaster risk reduction: Mitigation and preparedness in development and emergency programming. London: Overseas Development Institute.